# On Flowfield Periodicity in the NASA Transonic Flutter Cascade, Part I—Experimental Study

J. Lepicovsky
Dynacs Engineering Company, Inc., Brook Park, Ohio

E.R. McFarland, R.V. Chima, and J.R. Wood
Glenn Research Center, Cleveland, Ohio

Since its founding, NASA has been dedicated to the advancement of aeronautics and space science. The NASA Scientific and Technical Information (STI) Program Office plays a key part in helping NASA maintain this important role.

The NASA STI Program Office is operated by Langley Research Center, the Lead Center for NASA's scientific and technical information. The NASA STI Program Office provides access to the NASA STI Database, the largest collection of aeronautical and space science STI in the world. The Program Office is also NASA's institutional mechanism for disseminating the results of its research and development activities. These results are published by NASA in the NASA STI Report Series, which includes the following report types:

- TECHNICAL PUBLICATION. Reports of completed research or a major significant phase of research that present the results of NASA programs and include extensive data or theoretical analysis. Includes compilations of significant scientific and technical data and information deemed to be of continuing reference value. NASA's counterpart of peer-reviewed formal professional papers but has less stringent limitations on manuscript length and extent of graphic presentations.

- TECHNICAL MEMORANDUM. Scientific and technical findings that are preliminary or of specialized interest, e.g., quick release reports, working papers, and bibliographies that contain minimal annotation. Does not contain extensive analysis.

- CONTRACTOR REPORT. Scientific and technical findings by NASA-sponsored contractors and grantees.

- CONFERENCE PUBLICATION. Collected papers from scientific and technical conferences, symposia, seminars, or other meetings sponsored or cosponsored by NASA.

- SPECIAL PUBLICATION. Scientific, technical, or historical information from NASA programs, projects, and missions, often concerned with subjects having substantial public interest.

- TECHNICAL TRANSLATION. English-language translations of foreign scientific and technical material pertinent to NASA's mission.

Specialized services that complement the STI Program Office's diverse offerings include creating custom thesauri, building customized data bases, organizing and publishing research results . . . even providing videos.

For more information about the NASA STI Program Office, see the following:

- Access the NASA STI Program Home Page at *http://www.sti.nasa.gov*

- E-mail your question via the Internet to help@sti.nasa.gov

- Fax your question to the NASA Access Help Desk at (301) 621-0134

- Telephone the NASA Access Help Desk at (301) 621-0390

- Write to:
  NASA Access Help Desk
  NASA Center for AeroSpace Information
  7121 Standard Drive
  Hanover, MD 21076

# On Flowfield Periodicity in the NASA Transonic Flutter Cascade, Part I—Experimental Study

J. Lepicovsky
Dynacs Engineering Company, Inc., Brook Park, Ohio

E.R. McFarland, R.V. Chima, and J.R. Wood
Glenn Research Center, Cleveland, Ohio

National Aeronautics and
Space Administration

Glenn Research Center

March 2000

# Acknowledgments

Available from

| | |
|---|---|
| NASA Center for Aerospace Information | National Technical Information Service |
| 7121 Standard Drive | 5285 Port Royal Road |
| Hanover, MD 21076 | Springfield, VA 22100 |
| Price Code: A03 | Price Code: A03 |

# ON FLOWFIELD PERIODICITY IN THE NASA TRANSONIC FLUTTER CASCADE, PART I— EXPERIMENTAL STUDY

**J. Lepicovsky**
Dynacs Engineering Company, Inc.
Brook Park, Ohio 44142


**E.R. McFarland, R.V. Chima, and J.R. Wood**
National Aeronautics and Space Administration
Glenn Research Center
Cleveland, Ohio 44135

## ABSTRACT

An extensive study to improve flow uniformity and periodicity in the NASA Transonic Flutter Cascade is presented here. The results are reported in two independent parts dealing with the experimental approach and the analytical approach. The first part, the Experimental Study, focuses first on the data sets acquired in this facility in the past and explains several discrepancies, particularly the questions of actual flow incidence and cascade backpressure levels. Next, available means for control and modifications of the cascade flowfield, boundary layer bleed and tailboard settings are presented in detail. This is followed by experimental data sets acquired in modified test facility configurations that were based on analytical predictions of the cascade flowfield. Finally, several important conclusions about improving the cascade flowfield uniformity and blade load periodicity are summarized. The important conclusions are: (1) boundary layer bleed does not improve the cascade flow periodicity; (2) tunnel wall contours must be carefully matched to the expected shape of cascade streamlines; (3) actual flow incidence for each cascade configuration rather must be measured instead of relying on the tunnel geometry; and (4) the current cascade configuration exhibits a very high blade load uniformity over six blades from blade #2 to blade #7, and the facility is now ready for unsteady pressure data acquisition.

## INTRODUCTION

Modern turbofan engines employ a highly-loaded, low-aspect ratio fan stage with transonic or low-supersonic velocities in the blade-tip region. The tip-section airfoils of these fan blades are noticeably different from the airfoils on the rest of the blade.

The tip-section airfoils are designed for precompression, with a concave suction surface just downstream of the leading edge, and with very low overall camber. The airfoils have a sharp leading edge and are prone to flow separation at off-design conditions. Due to extreme flight envelope requirements, the engines are often operated near the stall flutter boundary of the fan, which occurs at high incidence angles and high subsonic or transonic relative Mach numbers. Blade flutter and associated high cycle fatigue problems are very detrimental to the engine health and must be avoided. Stall flutter and particularly blade life prediction codes are not yet fully reliable; their verification is hampered by a lack of reliable unsteady loading data, particularly for the airfoils in question. Therefore there has been great interest in fan blade stall flutter research in recent years.

Work at the NASA Glenn Research Center (GRC) on fan blade stall flutter has focused on improving the quality of experimental data acquired in the NASA Transonic Flutter Cascade Facility. The work was thematically organized into three groups. First, old data on symmetrical circular arc airfoils and initial data on transonic fan blade airfoils were carefully reviewed and analyzed with respect to the test facility performance. Then, the test facility configuration and its modifications were modeled computationally and the computational results analyzed. Finally, the test facility was modified accordingly and the experimental results were compared with the predictions. The results were analyzed for flow periodicity and flow uniformity. Computational and experimental work were sometimes run concurrently. The results achieved are described in two parts. The first paper, Experimental Study, presents the experimental effort. Computational work is presented in the second paper, Numerical Study, by Chima et al. (2000).

## NOMENCLATURE

| | | |
|---|---|---|
| C | [mm] | airfoil chord |
| $c_p$ | [1] | pressure coefficient |
| $F_B$ | [N] | resulting force on blade |
| h | [mm] | blade height |
| $i_{FL}$ | [dg] | flow incidence angle |
| $i_{GM}$ | [dg] | geometric incidence angle |
| Ma | [1] | Mach number |
| $p_w$ | [kPa] | wall static pressure |
| $p_{1t}$ | [kPa] | tunnel inlet total pressure |
| S | [mm] | blade pitch |
| $T_B$ | [Nm] | resulting torque on blade (to pivot point) |
| v | [m.s$^{-1}$] | cascade inlet velocity |
| W | [mm] | cascade test section width at $x/C = -0.355$ |
| x | [mm] | axial distance (cascade) |
| y | [mm] | pitchwise distance (cascade) |
| z | [mm] | spanwise distance (cascade) |
| $\Delta c_p$ | [1] | pressure coefficient deviation from blade #5 |
| $\gamma$ | [dg] | blade stagger angle (from axial direction) |
| $\lambda_T$ | [dg] | lower tailboard angle (from horiz. direction) |
| $\pi_{ET}$ | [1] | empty tunnel pressure ratio |
| $\pi_{TB}$ | [1] | cascade pressure ratio |
| $\rho$ | [kg.m$^{-3}$] | air density |
| $\theta$ | [dg] | leading edge camber angle (airfoil) |
| $\xi$ | [mm] | chordwise distance (airfoil) |

Index:

| | |
|---|---|
| 0 | far upstream |
| 1 | upstream |
| 2 | downstream |
| — | average value over the range $0.2 < y/W < 0.8$ |

Definitions:

Pressure coefficient
$$\overline{c_p} = \frac{p_\xi - \overline{p_1}}{0.5 \, \overline{\rho_1} \, \overline{v_1}^2}$$

Pressure ratio
$$\pi_{TB} = \overline{p_2} / \overline{p_1}$$

## PREVIOUS WORK ON NASA FLUTTER CASCADE

The NASA GRC Transonic Flutter Cascade is one of a very few test facilities dedicated to the unsteady aerodynamics of oscillating airfoils. The facility is used to provide data for modeling aerodynamics of blade stall flutter. The facility combines a linear cascade wind tunnel with a high-speed drive system that imparts pitching oscillations to cascade blades. The cascade consists of nine blades. All the blades or any single blade can be oscillated at realistic reduced frequencies (Strouhal numbers). Interblade phase angles can be varied in increments of 15 dg. The facility has been described in detail in works of Boldman and Buggele (1978), Shaw et al. (1986), and Buffum et al. (1996). Only features relevant to the current investigations will be emphasized here.

A schematic diagram of the original build of the NASA Transonic Flutter Cascade facility is given in Fig. 1. A close-up

photograph of the cascade test section is in Fig. 2. As seen in Fig. 1, the facility was provided with a complex bleed system that was intended to remove the boundary layer of the incoming flow and thus improve its uniformity. Fourteen independent valves were available to adjust the bleed -- two for the lower wall and lower scoop, two for the upper wall and upper scoop, and five valves for compartmentalized bleed manifolds on each (front and back) side wall. In addition, upper and lower tailboards allow angular adjustment for improving flow uniformity. A primary concern in this facility was to ensure uniformity of the flow ahead of the cascade, and periodicity of the flow within the cascade. It was hoped that tailboards and bleed control would help to achieve a high passage-to-passage blade load periodicity for steady flow conditions in the cascade.
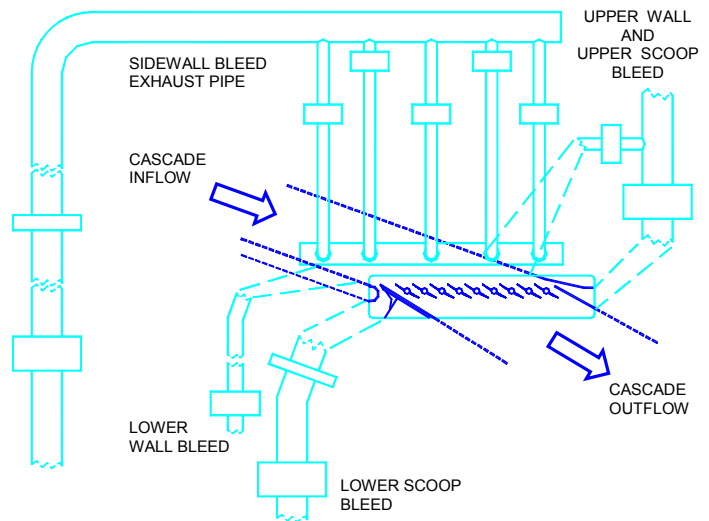


**Fig. 1 Boundary layer bleed system of the NASA Transonic Flutter Cascade facility**
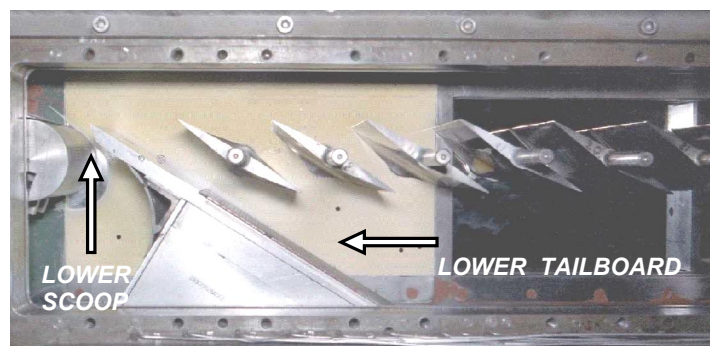


**Fig. 2 View of cascade test section**

In recent years, the facility has been used to investigate behavior of a cascade of modern, low-aspect ratio fan blades operating near the stall flutter boundary that occurs at high incidence angles and high subsonic and transonic relative Mach numbers. The blades for this experiment were designed and manufactured by Pratt&Whitney Engine Company. The airfoil

and cascade parameters are given in Fig. 3 and Tab. 1 (Buffum et al., 1996a). Previous measurements on these blades were reported by Buffum et al. (1996a, 1996b) at Mach numbers between 0.5 and 0.8, and chordal, geometric incidence angles, $i_{GM}$, of 0 and 10 dg. Experimental blade-surface pressure distributions for steady flow at inlet Mach numbers of up to 0.5 were compared with various CFD predictions (Buffum et al., 1996a, 1996b), but good agreement was found only up to 85% of chord and only for the incidence angle of 0 dg. The cascade flow periodicity was measured only for the three middle blades and was found sufficient for unsteady surface-pressure data sets acquired at full-chord reduced frequencies of 0.4 and 0.8, and for an interblade phase angle of 180 dg.
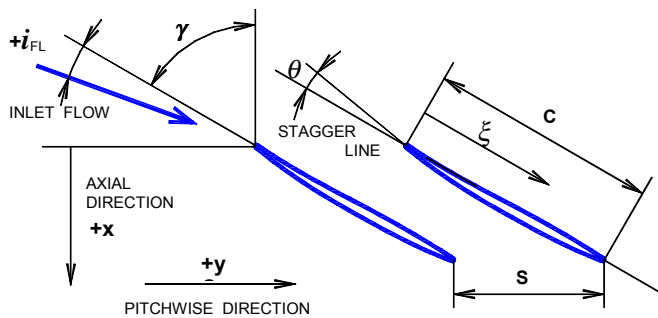


**Fig. 3   Airfoil and cascade coordinate system**

| Blade chord, | C | 89.2 |
|---|---|---|
| Leading edge camber angle, | $\theta$ | $-9.5$ dg |
| Maximum thickness, | $t_{max}$ | 0.048 C |
| Location of maximum thickness, | $\xi_{max}$ | 0.625 C |
| Stagger angle, | $\gamma$ | 60.0 dg |
| Number of blades in the cascade, | | 9 |
| Blade pitch, | S | 58.4 mm |
| Cascade solidity, | C/S | 1.52 |
| Pitching axis, | $\xi_{ax}$ | 0.5 C |
| Blade height, | h | 95.9 mm |

**Tab. 1   Airfoil and cascade parameters**

## UNRESOLVED PROBLEMS WITH FLUTTER CASCADE DATA

The unsteady data, reported by Buffum et al. (1996a, 1996b), were acquired for oscillations of all nine blades. The older work done in this cascade (Buffum and Fleeter, 1991) reported that the oscillating cascade produced waves which for some interblade phase angles reflected off the wind tunnel walls back into the cascade and interfered with the cascade unsteady aerodynamics. Later, the tunnel was provided with perforated walls at several locations and acoustic treatment. The efficiency of this arrangement still has not been proven. Ott at al. (1998) recommended for their facility just the opposite: replacement of slotted walls with solid ones.

To ease the facility operation, it was decided to adopt a method of influence coefficients for the future unsteady work in this cascade. For the unsteady influence coefficient technique, only one blade in the cascade is oscillated at a time and the resulting unsteady pressures are measured on the remaining (nonmoving) blades. The unsteady aerodynamics of an equivalent cascade with all blades oscillating at a specified interblade phase angle are then determined through a vector summation of unsteady data from individual blades (Buffum and Fleeter, 1988). It must be stated that the use of the influence coefficient technique has only been demonstrated for attached flow. This facility has the unique capability of demonstrating this technique for separated flow. This technique requires a high degree of flow periodicity within the cascade for a larger number of blades. It was decided to investigate all means available in the test facility to broaden the range of good flow periodicity beyond the three middle blades.
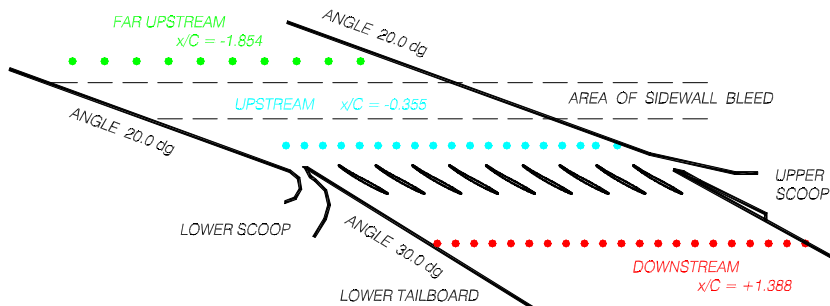
Another problem was establishing the actual value of the flow incidence angle in the cascade. The previous work always reported the geometric incidence angle, $i_{GM}$, based on the facility configuration. Actual flow incidence, $i_{FL}$, just upstream of the cascade was not measured. Frequent comments from the CFD community were that to achieve reasonably good agreement between the measured steady state pressure distribution on the blades and predicted distributions, the incidence angle for the CFD calculations had to be lowered by about 1.5 to 2.5 dg at the high incidence case. In addition, pressures measured downstream of the cascade were generally inconsistent with CFD predictions. Both of these discrepancies are addressed here.

## TECHNICAL APPROACH TO IMPROVING CASCADE FLOW QUALITY

The approach to resolving reported discrepancies was at first focused on experimental work only. The inlet duct was instrumented with additional side-wall static taps. Flow visualization and pressure sensitive paint (PSP) techniques were employed to assess the flow periodicity in the cascade. A variety of bleed conditions and tailboard settings were investigated. The flow uniformity was judged by evaluating the results of detailed measurements of sidewall static pressures: far upstream, upstream, and downstream of the cascade. Measurement of flow incidence angle and exit flow parameters were also performed. This effort, however, resulted in minor improvements only. It became obvious that there is a fundamental mismatch between the tunnel test section configuration and blade cascade performance resulting in a strong wall tunnel interference with the cascade flowfield. All subsequent modifications and changes were based on analytical predictions of the complete tunnel flowfield provided by McFarland, and cascade flow analysis provided by Chima. The analytical approaches of McFarland and Chima are described in detail in the second part of this paper (Chima et al., 2000). Only experimental results are reported in this part of the paper.

For easy orientation the three distinct configurations of the cascade facility, discussed in this paper, were labeled *C_20.0 / 30.0*, *C_21.5 / 24.5*, and *C_20.0 / 24.0*, where the first number indicates inlet wall angle, and the second number is the angle of the exit wall. The wall angles are measured from the horizontal direction.



**Fig. 4. Cascade configuration *C_20.0 / 30.0***



**Fig. 5. Effects of sidewall boundary layer bleed rate**



**Fig. 6. Effects of lower scoop bleed rate for inlet Mach number of 0.8**

A rigorous way to determine the flow periodicity is to compare the pressure loadings of all blades in the cascade. However, only two blades are fully instrumented with 15 static taps at the blade midspan height -- one blade with instrumented suction side and the other one with instrumented pressure side. Consequently, the instrumented blades must be marched along the cascade, which is a time consuming procedure. Therefore, initially, the focus was on uniformity of sidewall pressure distributions, mainly upstream and downstream of the cascade. The main goal was to find a facility configuration that would exhibit uniform wall static pressure distributions in the cascade region.
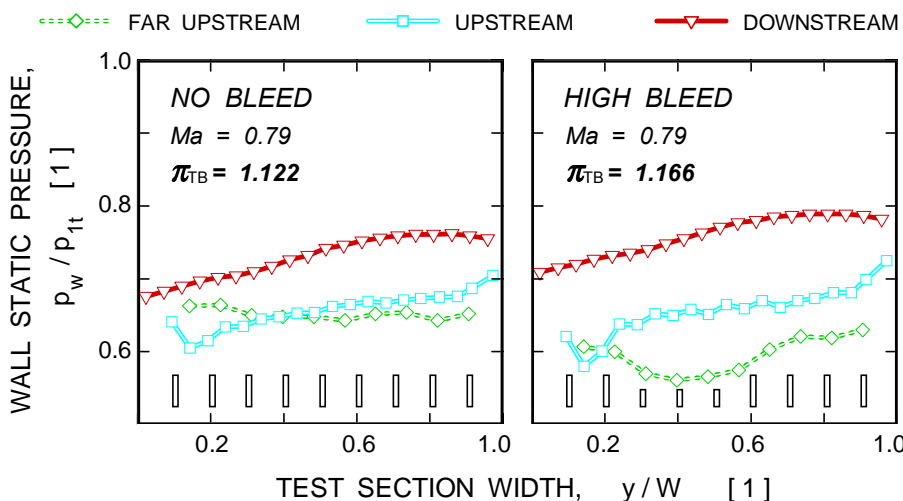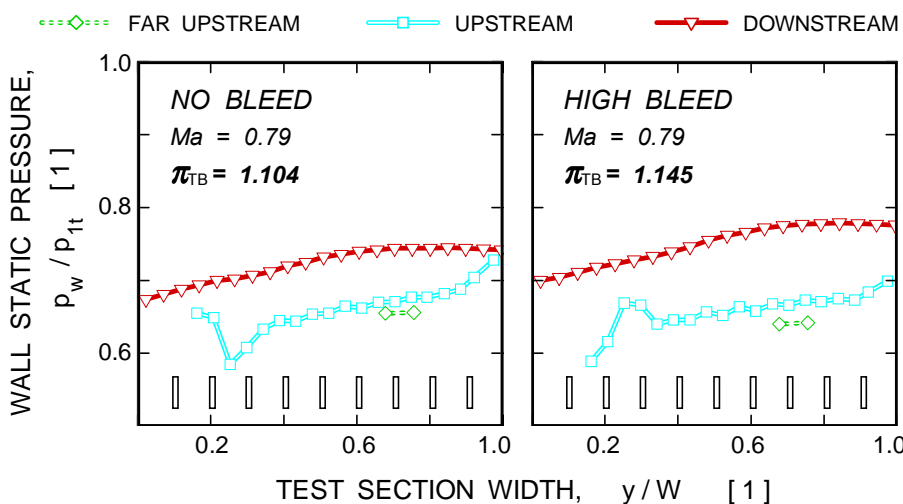
## CASCADE CONFIGURATION *C_20.0 / 30.0*

### Effects of bleed rate and lower tailboard setting (*C_20.0 / 30.0*)

A schematic diagram of cascade configuration *C_20.0 / 30.0* is shown in Fig. 4. This was the original build of the NASA flutter cascade. The first step in the current investigation was to explore the effects of available controls (bleed system and adjustable tailboards) on the uniformity of flow in the test facility. The flow uniformity was judged based on pitchwise distributions of wall static pressures at three measurement stations: far upstream ($x/C = -1.854$), upstream ($x/C = -0.355$), and downstream ($x/C = +1.388$) of the cascade. The measurement stations are indicated in Fig. 4; the dimensionless axial distance from the cascade leading-edge plane, $x/C$, is based on the blade chord. It should be mentioned that the rows of static taps far upstream and upstream of the cascade are on the back side wall, while the downstream row of static taps is on the front side wall.

Figure 5 shows the wall static pressures for no and high sidewall bleeds (about 15% of the total mass flow). All three pressure distributions are plotted with respect to the test section width (W = 613 mm). The location of the cascade blades is also indicated in the figure. The cascade inlet Mach number was 0.8. The inlet Mach number was determined from the average static pressure upstream of the cascade at $x/C = -0.355$ (using static taps in the range $0.2 < y/W < 0.8$) and the total pressure at the inlet into the test facility. As seen in Fig. 5, bleed significantly affects the static pressure
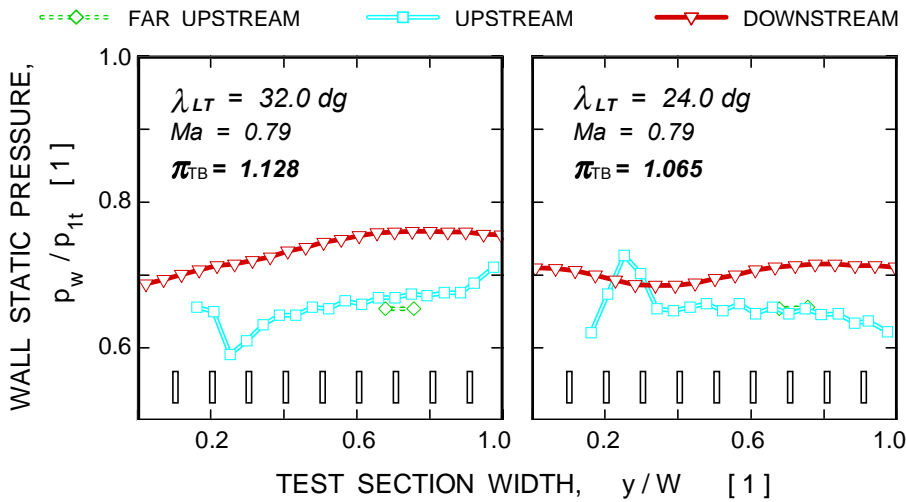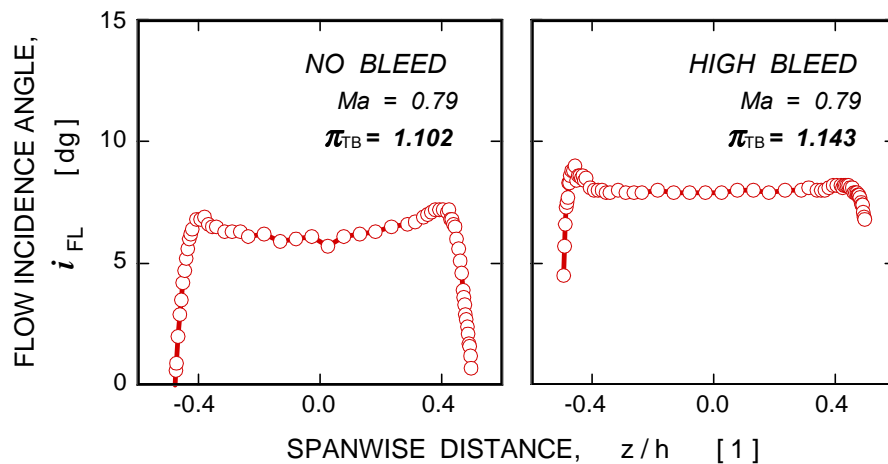
**Fig. 7. Effects of setting angle of the lower tailboard**
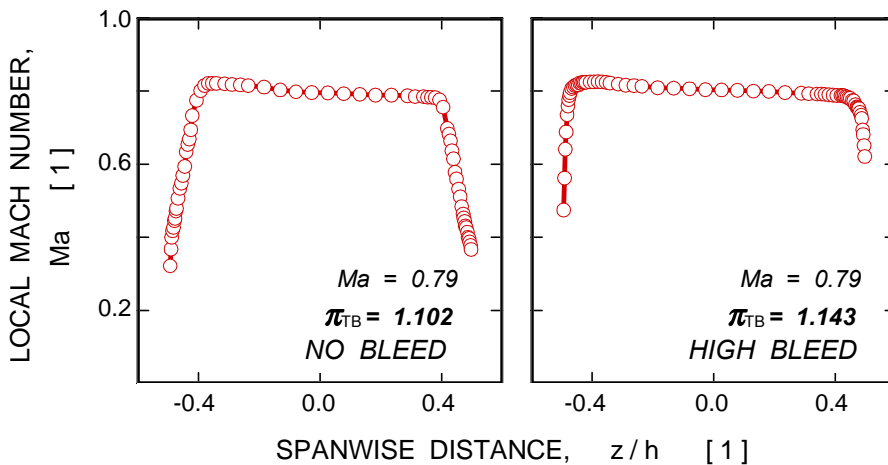


**Fig. 8. Effects of sidewall bleed on spanwise Mach number distribution at y/W = 0.388 and x/C = −0.254**



**Fig. 9. Effects of bleed on spanwise distribution of flow incidence angles at y/W = 0.388 and x/C = −0.254**

far upstream of the cascade and to a small degree also the average pressure ratio over the cascade ($\pi_{TB}$ = 1.122 versus $\pi_{TB}$ = 1.166). In both cases, however, the cascade is subjected to nonuniform inlet flow that decreases from Ma = 0.86 on the left-hand side to Ma = 0.73 on the right-hand side of the cascade. Sidewall bleed did not improve the incoming flow uniformity.

The effects of lower-scoop bleed are shown in the Fig. 6. For no lower-scoop bleed, the upstream static pressure distribution exhibits a pressure rise in the lower-scoop vicinity (left-hand side of the plot). For high lower-scoop bleed, the flow close to the lower scoop is noticeably accelerated (the lower scoop bleed is a local sink) which is manifested by the local pressure minimum in the scoop region. In any case the effects of lower-scoop bleed are restricted to a small region and do not affect the bulk of the cascade inlet flow.

Finally, the effects of lower tailboard angle setting are shown in Fig. 7. When the lower tailboard was pitched to $\lambda_T$ = 32.0 dg angle (diverging exit channel), the local minimum on the left side of the upstream static pressure distribution deepened; when the same tailboard was set to $\lambda_T$ = 24.0 dg (converging exit channel) a distinct pressure peak appeared on the left side upstream of the cascade. A probable reason for the peak was that the lip of the lower scoop now protruded into the flow (the tailboard pivot point is 45 mm downstream of the tailboard tip). More importantly, there was also a noticeable effect on the downstream pressure distribution that became more uniform; however, the pressure distribution was now sloped from left to right which indicated increasing loading of the blades from left to right. This exercise indicated that the tunnel flow exit direction, forced on the flow by the original tailboard setting to $\lambda_T$ = 30.0 dg, did not properly match the cascade exit flow angle. A proper match of the flow and tailboard angles was incorporated in the new facility configurations as discussed later.

In summary, none of the above controls used -- boundary layer bleed or setting the left tailboard alone -- substantially improved overall uniformity of the cascade static pressure field. The changes observed were mostly of local character.

## Spanwise Mach number and flow incidence (C_20.0 / 30.0)

The next series of experiments was aimed at measuring spanwise distributions of the upstream Mach numbers and flow angles directly using a traversing cobra probe. The effects of bleed on these distributions were also measured. The facility is provided with five upstream ports for spanwise traversing at $x/C = -0.254$. Results of these measurements are presented in Figs. 8 through 10.

As mentioned above, the test conditions were always set for a selected upstream inlet Mach number regardless of the bleed rate. Therefore, the effects of bleed on spanwise Mach number profiles are only manifested by changes in the thickness of the wall boundary layer (Fig. 8). However, the pressure ratio over the cascade is noticeably effected by the rate of bleed ($\pi_{TB} = 1.102$ versus $\pi_{TB} = 1.143$). Further, the rate of boundary layer bleed also noticeably affects the true incidence angle $i_{FL}$. In the previous investigations by Buffum et al. (1996a, 1996b), the stated incidence angle was the geometric incidence angle $i_{GM}$ (difference between the inlet duct wall direction and the stagger angle of the blades). As will be shown below, in most cases the geometric incidence angle differs from the true flow incidence. Fig. 9 shows the spanwise distributions of the flow incidence angles without bleed and with high bleed as measured at $y/W = 0.388$ for the geometric incidence of 10.0 dg. As seen here, the midspan flow incidence angle is less than the geometric incidence for both cases; 6.2 dg for no bleed, and 8.1 dg for the high bleed rate. Finally, Fig. 10 shows the midspan flow incidence angle at four locations along the cascade width for inlet flow Mach numbers of 0.5 and 0.8. The experiments of Buffum et al. were carried out for the three middle blades (#4, #5, and #6). In this region ($0.4 < y/W < 0.6$) the flow incidence varies by 2 to 3 dg across the blade passages, and it is always smaller (by 1.5 to 2.5 dg) for the no bleed case than it is for the case of the high bleed rate. Buffum did not report the bleed rate involved but there are indications that it was not very high; consequently, it can be safely assumed that the actual flow incidence angle for Buffum's data was between 7.5 to 9.0 dg. This assumption seems to be confirmed by CFD results of Chima et al. (2000), where the best fit of calculated blade loading diagrams with data of Buffum et al. (1996a, 1996b) was achieved for incidence angles about 8 dg.

## Blade loading and flow periodicity (C_20.0 / 30.0)

The effects of boundary layer bleed rate on blade loading diagrams are shown in Fig. 11. The difference for no-bleed and high-bleed conditions is obvious. An unspecified, and possibly non repeatable bleed, can alter the experimental data significantly. Because this cascade will also be used for flutter experiments in transonic flows, several tests for transonic flow operating conditions were also carried out. Boundary layer bleeding significantly altered the shock wave pattern in the cascade as shown by shadowgraph images in Fig. 12. The shadowgraph pictures were obtained using a dedicated double-pass schlieren system as described by Boldman and Buggele (1983).

Finally, Fig. 13 illustrates periodicity of the cascade flowfield for an inlet Mach number of 1.35 with high bleed. A shadowgraph picture of the cascade shock structure is acompanied by a sidewall static pressure field acquired using the technique of pressure sensitive paints as described by Bencic (1995) and Lepicovsky at al. (1997).
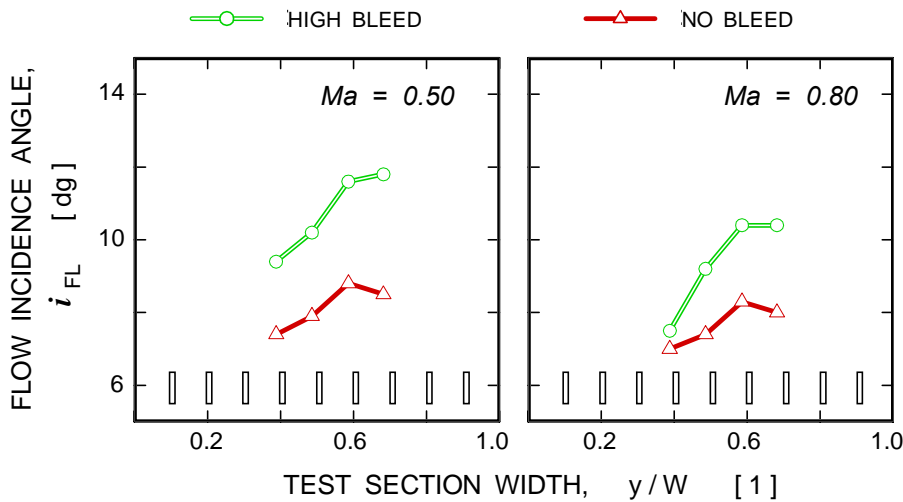


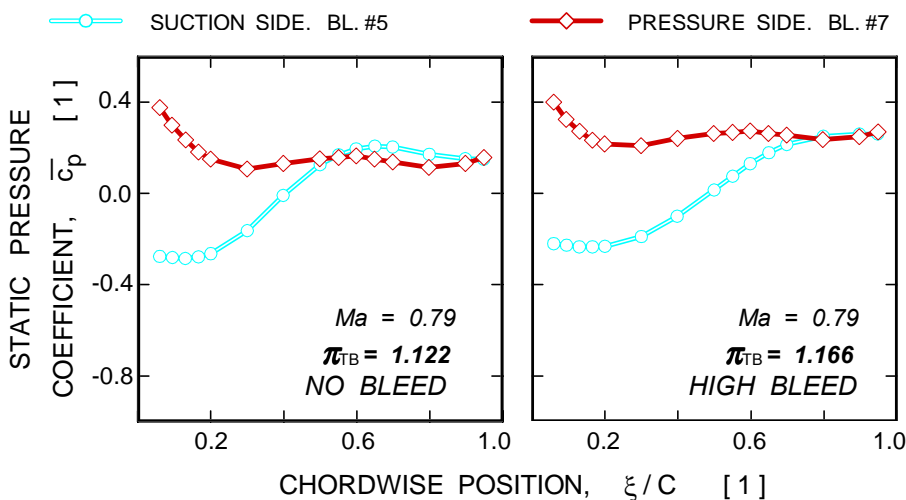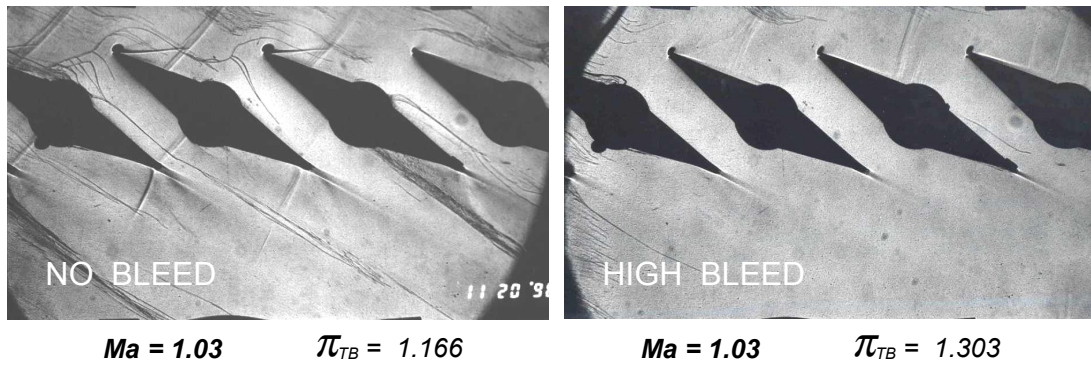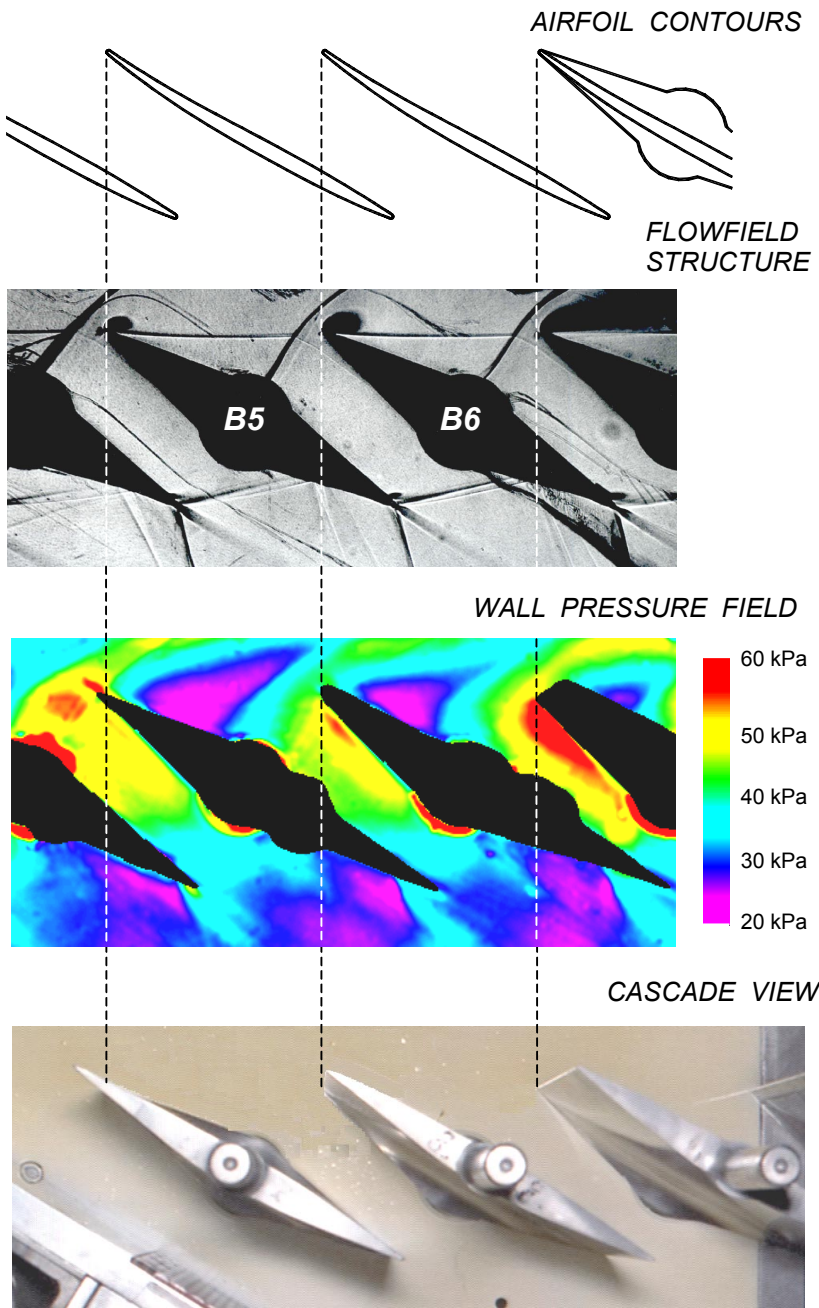**Fig. 10.    Effects of bleed on pitchwise distribution of flow incidence angles**



**Fig. 11.        Effects of bleed rate on blade loading**

NO BLEED       HIGH BLEED

$Ma = 1.03$    $\pi_{TB} = 1.166$      $Ma = 1.03$    $\pi_{TB} = 1.303$

**Fig. 12   Effects of sidewall bleed rate on shock-wave pattern for an inlet Mach number of 1.03**

It can be observed here, that a periodic shock structure is in a flowfield which exhibits an overall positive pressure gradient in the pitchwise direction from the left end of the cascade to the right. The increasing pressure gradient across the cascade is manifested by decreasing relative depth of wall pressure depressions above the blades just past the blade leading edges. The slope of the sidewall pressure gradient is consistent with data presented in Fig. 5.

It is obvious from the previous results that boundary layer bleed noticeably affects the uniformity of the flow incidence angle ahead of the cascade (Figs. 9 and 10). Variations in the flow incidence cause non uniform blade loadings (Fig. 11). As demonstrated in Fig. 8, the Mach number profile at the midspan section of the channel, where most of the data is collected, is not affected by boundary layer bleed. Consequently, a decision was made not to use the cascade bleed system for the future experiments.

**Empty tunnel data (C_20.0 / 30.0)**

For the last experiment with this configuration, all blades were removed and wall static pressures were measured for the empty tunnel. The results are shown in Fig 14 for the inlet flow Mach numbers of 0.5 and 0.8. The distributions are very similar to those with blades in the tunnel (Fig. 5). This result confirmed that the flowfield in this cascade configuration was driven mainly by the tunnel walls and that the cascade had a very little effect here. Obviously, the turning angle imposed by the tunnel walls on the flow was significantly larger than the flow turning generated by the cascade. Similar results were predicted using McFarland's panel code, and are discussed in the second part of this paper (Chima et al., 2000).
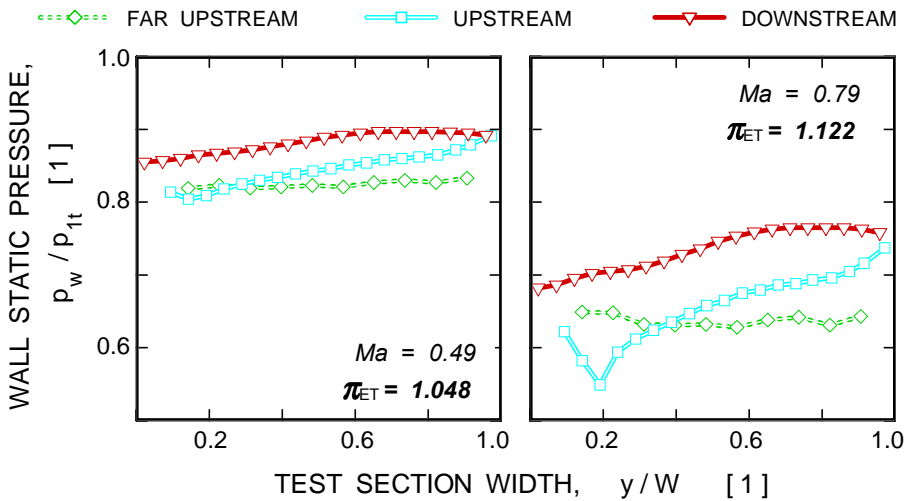


AIRFOIL CONTOURS

FLOWFIELD STRUCTURE

WALL PRESSURE FIELD

60 kPa
50 kPa
40 kPa
30 kPa
20 kPa

CASCADE VIEW

**Fig. 13.   Cascade Flowfield for Mach Number 1.35**

**Fig. 14.** Wall pressure distributions in an empty tunnel for configuration *C_20.0 / 30.0*

## CASCADE CONFIGURATION *C_21.5 / 24.5*

The next cascade configuration was based on calculation of the cascade turning angle using Chima's viscous code (Chima et al., 2000). We tried to maintain a flow incidence angle similar to the actual flow incidence as measured for the previous cascade configuration C_20.0 / 30.0. previous data set; therefore we selected the flow incidence of 8.5 dg. For this incidence, the cascade turning angle was expected to be about 3 dg. Consequently, the inlet duct was set to an angle of 21.5 dg and the exit tailboards were set to 24.5 dg. This cascade configuration, denoted C_21.5 / 24.5, is depicted in Fig. 15 (W = 607 mm).

### Wall static pressure distributions (C_21.5 / 24.5)

First data sets were obtained for the empty tunnel; the results for inlet Mach numbers of 0.5 and 0.8 are shown in Fig. 16. The static pressure field was quite uniform along the cascade width. This was a very encouraging result. When the blades were placed back in the tunnel, the downstream static pressure distribution remained flat; however, the upstream static pressure field exhibited a sudden increase at the left-hand end of the cascade (Fig. 17). The possibility that this pressure rise was

caused by flow blockage in this cascade section due to the proximity of the first blade to the tunnel left wall (Fig. 15) was considered. McFarland's prediction of the cascade static pressure field (Chima et al., 2000) indicated that there is a pressure disturbance propagating from the first blade upstream of the cascade. The predicted location of this disturbance at the station of the upstream static taps coincided reasonably well with the measured data. To verify this prediction, we removed the first blade of the cascade and repeated the experiment. The result is in Fig. 17 (right-hand plot). The location of the upstream static pressure increase moved one blade pitch to the right, exactly as predicted by McFarland. The calculations and comparisons with experimental data are discussed in the second part of this paper (Chima et al., 2000).

### Blade loading and flow periodicity (C_21.5 / 24.5)

Blade loading periodicity was verified by measuring load diagrams for all blades in the cascade. As mentioned above, we had only two blades instrumented with static taps at the blade midspan, and consequently these two blades had to be 'marched' through the cascade. We kept tunnel operation conditions repeatable within 1% of the inlet Mach number for each blade position. Two of the loading diagrams for instrumented blade positions 4+5 and 5+6 are shown in Fig. 18.

To visualize differences in loading diagrams for individual blades, we plotted differences between pressure coefficient values of a particular blade and the blade in position #5. The plots of measured differences (pressure coefficient deviations) are shown in Fig. 19 for an inlet Mach number of 0.8. First, the sketch at the top of the figure identifies individual blades with color coded numbers. The left half of the cascade consists of blades 1 through 5 and the right half of blades 5 through 9. Of the four plots in Fig. 19, the two on the left are for the cascade left half, the two on the right are for the cascade right half, the two lower plots show data for blade pressure surfaces. As mentioned above, the blade differences with respect to blade #5 are plotted here. Blade #5 is represented by a straight, black, broken line. The actual loading diagram for blade #5 can seen in Fig. 18. The deviation curves for the remaining blades in Fig. 19 are color coded in accordance with the blade numbers in the sketch. For a perfectly periodic flow in the cascade, all deviation curves would collapse to the broken straight line of blade #5. Positive values of deviation indicate that a particular blade has, at that chordwise position, a higher pressure coefficient value than the blade #5 at the same chord station.
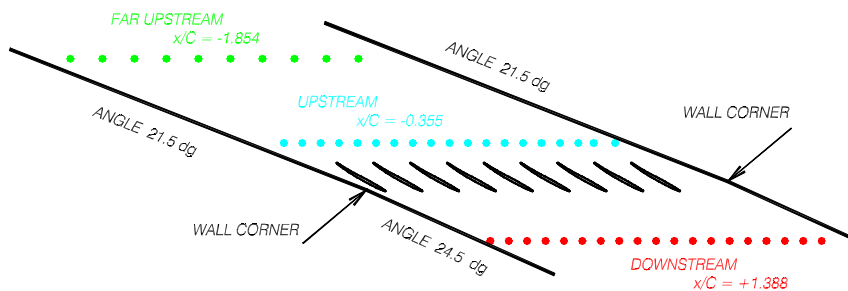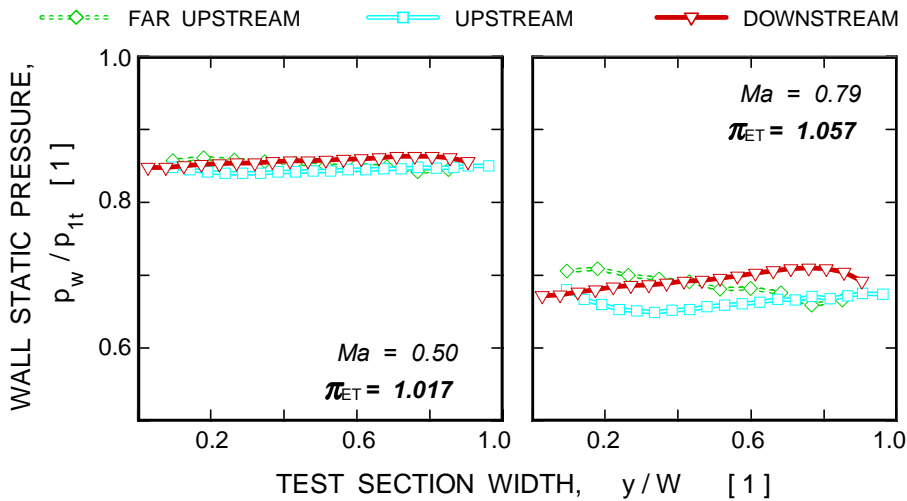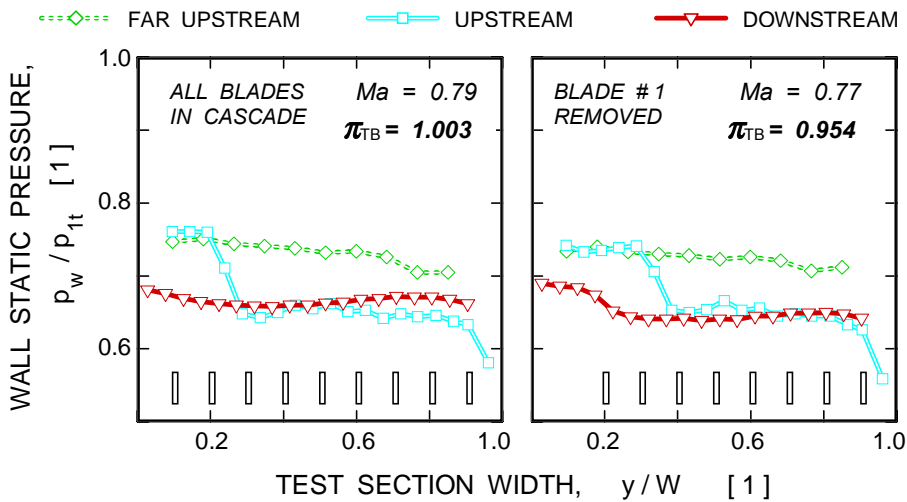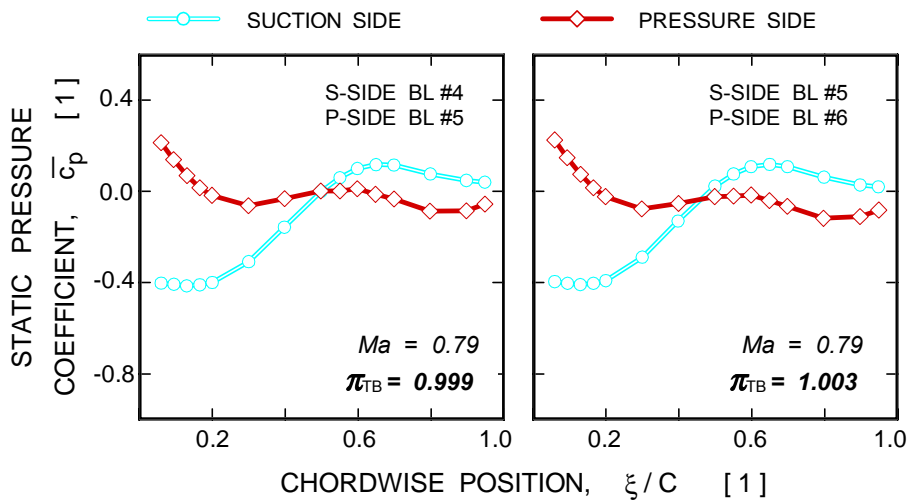


**Fig. 15.** Cascade configuration *C_21.5 / 24.5*

**Fig. 16. Wall pressure distributions in an empty tunnel for configuration C_21.5 / 24.5**



**Fig. 17. Effect of the first blade on wall pressure for configuration C_21.5 / 24.5**



**Fig. 18. Blade loading diagrams for configuration C_21.5 / 24.5**

For a negative deviation value, the pressure coefficient of a particular blade is smaller than that on blade #5.

A comment must be made here about the measuring accuracy. All pressures in the cascade were measured with absolute pressure transducers with a range of 100 kPa (15 psia), and an accuracy better than ±0.4%. This translates to an accuracy of ±0.02 for the value of pressure coefficient. Therefore, it is reasonable to expect that deviations of pressure coefficient less than 0.04 may be considered as insignificant. In light of this, there is very good agreement in loading for suction surfaces of blades #4 and 5, while blade #6 is marginal. On the pressure side, the agreement is very good for blades #3, 4, 5, and 6, and marginal for blade #7.

Finally, the distribution of blade force and torque along the cascade is shown in Fig. 20. These quantities were integrated from the measured blade surface pressures. The blade force direction was perpendicular to the blade's chord. The blade torque was calculated relative to the chord midpoint. As seen here, the blade loading is not uniform. The first and the last blades are highly loaded with respect to the other blades. Surprisingly, the right half of the cascade is less loaded than expected. A comparison with predicted data is discussed in the second part of this paper (Chima et al., 2000).

Overall results from this cascade configuration indicated a slight improvement in comparison with the original configuration, however, the flow periodicity and uniformity was still not satisfactory. The major problem with this configuration was that we were unable to obtain transonic inlet flow in the cascade. The maximum inlet Mach number was 0.9. To obtain supersonic inlet flow in the tunnel we had to 'close' the inlet duct which was done by returning back to the headboard angle of 20 dg as discussed in the next section.

**Configuration C_21.5 / 24.5**

Ma = 0.79

$\pi_{TB}$ = 0.990
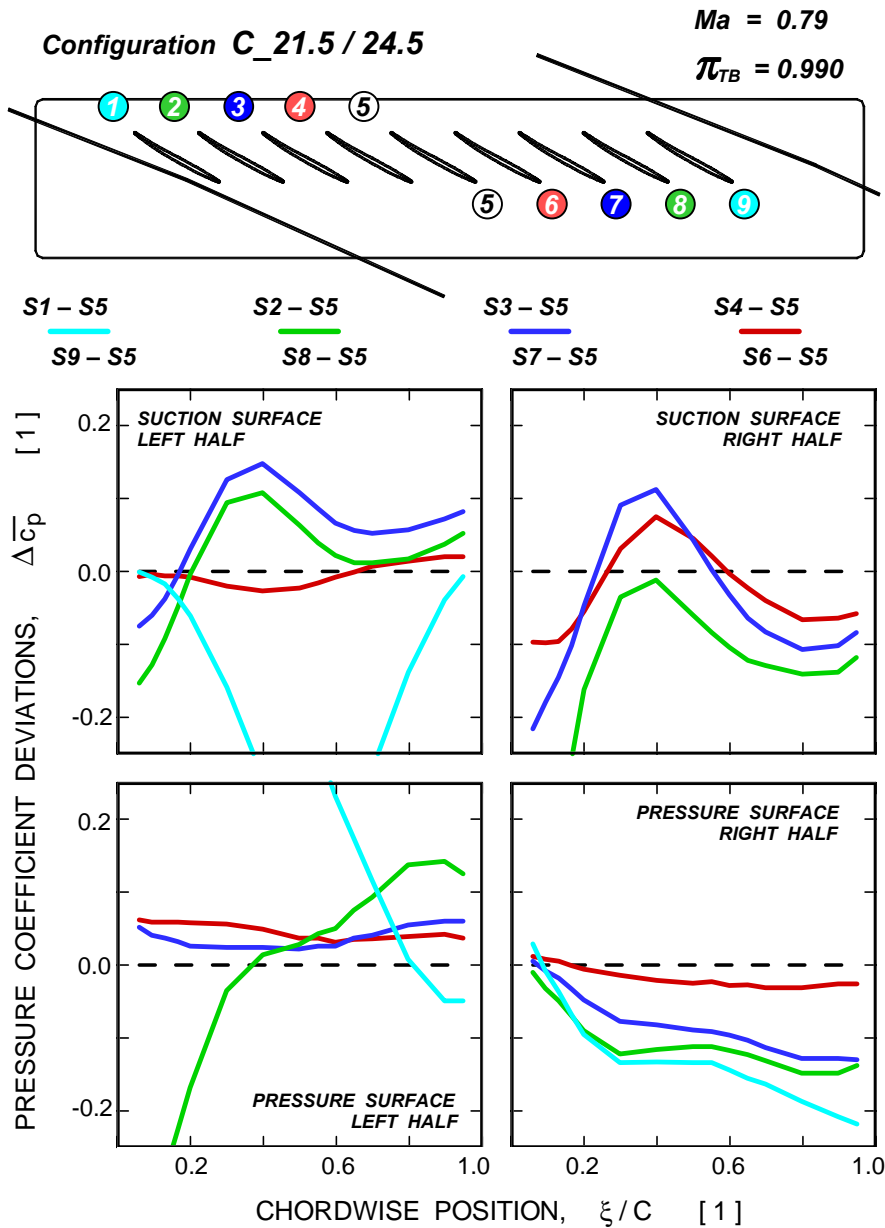


## Wall static pressures distributions (C_20.0 / 24.0)

Wall static pressures distributions for this configuration were very uniform as shown in Fig. 22 for three inlet Mach numbers of 0.5, 0.8, and 1.0. The saw tooth character of the upstream pressure distribution for Ma = 1.0 indicates presence of shock waves emanating from the blade leading edges. The uniformity of wall static pressures in the pitchwise direction was a good indicator of an improved cascade flow periodicity for this configuration.

## Blade loading and flow periodicity (C_20.0 / 24.0)

Blade loading diagrams for blade #4 (suction surface), blade #5 (suction and pressure surfaces) and blade #6 (pressure surface) for three inlet Mach number of 0.5, 0.8, and 1.0 are shown in Fig. 23. The first inspection reveals that there are no significant differences in pressure distributions for lower Mach numbers of 0.5 and 0.8. The loading diagrams for the inlet Mach number of 1.0, however, indicate changes in the flow pattern as the flow becomes transonic.

**Fig. 19.** Blade loading periodicity for configuration C_21.5 / 24.5

**Fig. 20.** Distribution of blade force and torque for configuration C_21.5 / 24.5
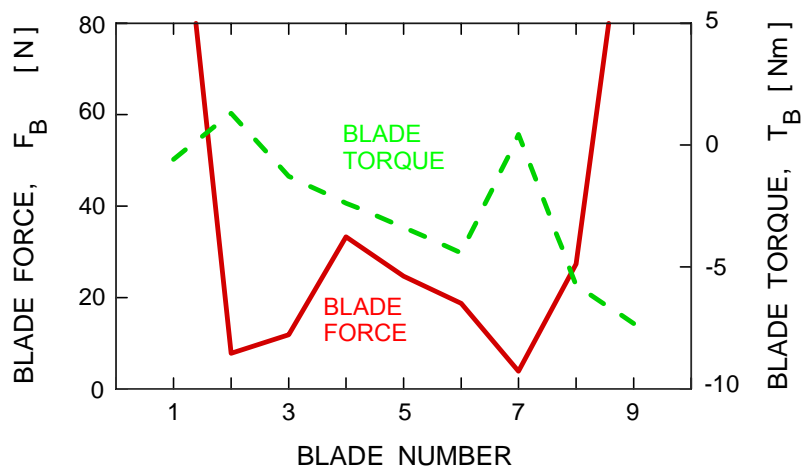
## CASCADE CONFIGURATION C_20.0 / 24.0

The final cascade facility configuration was based on R. Chima's suggestion to adjust the tunnel wall to the shape of *midpitch* streamlines of a perfectly periodic cascade. The configuration is shown in Fig. 21. The headboards were set to an angle of 20 dg, and the tailboards were set to 24 dg angle because CFD results showed the cascade turns the flow by 4 dg for the flow incidence angle of 10 dg. The headboards and tailboards were joined by an insert aligned with the blade setting angle of 30 dg. This insert approximated the streamlines at blade passage midpitch. The cascade width was W = 526 mm.
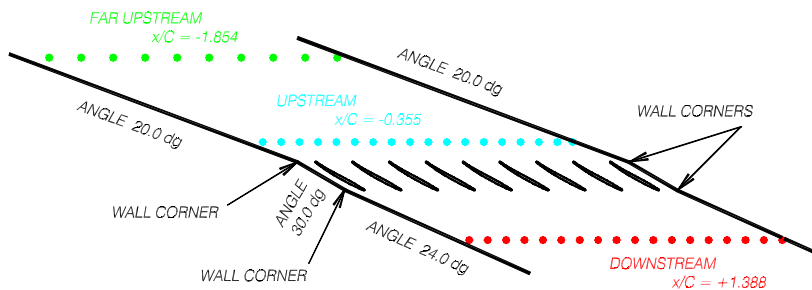
Fig. 21. Cascade configuration **C_20.0 / 24.0**

## CONCLUSIONS

A detailed experimental study, guided by CFD predictions, was carried out to improve flow uniformity and periodicity in the NASA Transonic Flutter Cascade. In the study, available means for control and modifications of the cascade flowfield were fully investigated and analyzed. Further, several discrepancies in the older data sets acquired were explained, particularly the questions of actual flow incidence angles and the inconsistency between predicted and measured backpressure levels. Several conclusions important for future work on unsteady pressure distributions in a cascade under stall flutter conditions were reached. The most important conclusions can be summarized as follows:

Blade loading periodicity was verified by measuring loading diagrams for all blades for this cascade configuration. Again the differences in loading diagrams for individual blades were plotted as differences between pressure coefficient values of a particular blade and the blade in position #5. The resulting plots of pressure coefficient deviations for an inlet Mach number of 0.8 are shown in Fig. 24. The structure of the figure is similar to that in Fig. 19. Significant improvements in the cascade flow periodicity for this cascade configuration are readily visible. Blades #2 through #5 in the left half of the cascade show excellent agreement of pressure distributions for the suction surface. Blades #5 through #7 in the right half show acceptable agreement in their suction side pressure distributions. On the pressure side, the agreement is excellent for blades #2 through #8. This is a very satisfactory result confirming the range of excellent flow periodicity in the cascade for six blades (#2 through #7). This result is also confirmed by blade force and torque distributions for this cascade configuration as shown in Fig. 25. On comparing this data with the data for the previous configuration ( see Fig. 20), large improvements toward loading uniformity are obvious for both force and torque distributions.

1.  The boundary-layer bleed did not improve the flowfield uniformity and blade-load periodicity of the cascade tested. On the contrary, high bleed affected pitchwise distribution of flow incidence angles along the cascade and thus contributed to blade load variations.
2.  The boundary layer bleed improves flow uniformity in the spanwise direction only in the vicinity of both sidewalls. The midspan section of the blade is not affected at all. For future experiments, it is recommended that the boundary-layer bleed system not be used.
3.  The tailboard setting significantly affects the pitchwise distribution of static wall pressures and their levels.
4.  It is extremely important to match the tunnel wall contours with expected streamlines. This is particularly important for conditions of blade separated flows where it may not be readily obvious. Any mismatch between the cascade streamlines and tunnel contour walls results in a tunnel driven flow with the cascade under investigation having very little effect on the flowfield.
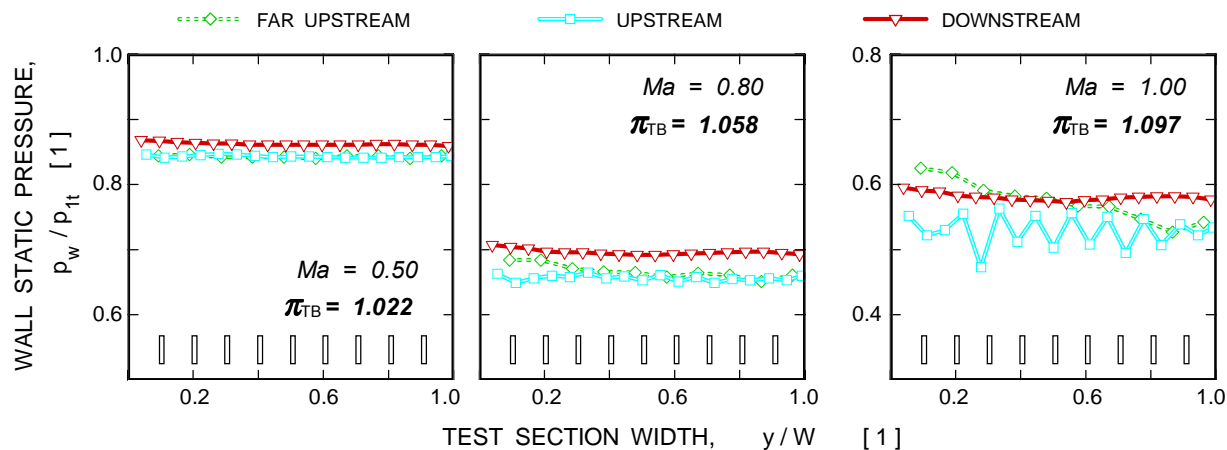


Fig. 22. Wall static pressure distributions for cascade configuration **C_20.0 / 24.0**

5. Flow incidence angles should be measured for each new configuration of the cascade facility. It is very risky to rely on geometric angles in determining the actual flow incidence.

6. By carefully tailoring tunnel wall contours to the expected streamlines for the current flow incidence of 10 dg, the flowfield uniformity upstream and downstream of the cascade improved significantly. Further, a very high blade load uniformity now extends over six blades from blade #2 to blade #7.

7. The facility is now ready for unsteady pressure data acquisition to acquire benchmark data sets for validating unsteady computational fluid dynamics codes used to model cascade stall flutter.

## REFERENCES

Bencic, T.J., 1995, "Experience Using Pressure Sensitive Paint in NASA Lewis Research Center Propulsion Test Facilities", AIAA Paper 95-2831.

Boldman, D.R. and Buggele, A.E., 1978, "Wind Tunnel Tests of a Blade Subjected to Midchord Torsional Oscillations at High Subsonic Stall Flutter Conditions", NASA TM-78998.

Boldman, D.R. and Buggele, A.E., 1983, "Experimental Evaluation of Shockless Supercritical Airfoils in Cascade", AIAA Paper 83-0003.

Buffum, D.H. and Fleeter, S., 1988, "Investigation of Oscillating Cascade Aerodynamics by an Experimental Influence Coefficient Technique", NASA TM-101313.

Buffum, D.H. and Fleeter, S., 1991, "Wind Tunnel Wall Effects in a Linear Oscillating Cascade", NASA TM-103690.

Buffum, D.H., Capece, V.R., King, A.J., and El-Aini, Y.M., 1996a, "Oscillating Cascade Aerodynamics at Large Mean Incidence", ASME Paper 96-GT-339; also NASA TM-107247.
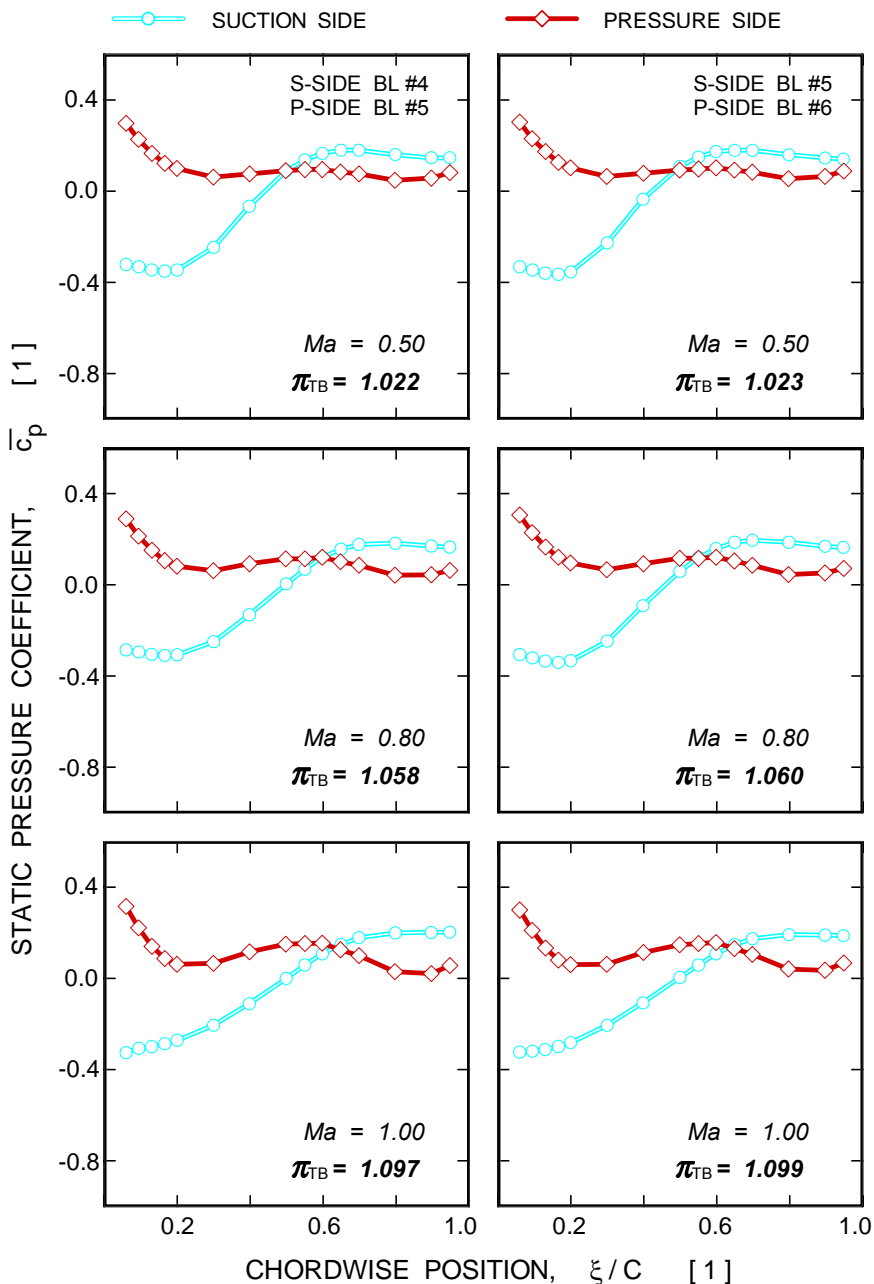
Buffum, D.H., Capece, V.R., King, A.J., and El-Aini, Y.M., 1996b, "Experimental Investigation of Unsteady Flows at Large Incidence Angles in a Linear Oscillating Cascade", AIAA Paper 96-2823, 1996; also NASA TM-107283.

Chima, R.V, McFarland, E.R., Wood, J.R., and Lepicovsky, J., 2000, "On Flowfield Periodicity in the NASATransonic Flutter Cascade, Part II – Numerical Study", ASME Paper 2000-GT-0573.

Lepicovsky, J., Bencic, T.C., and Bruckner, R.J., 1997, "Application of Pressure Sensitive Paint to Confined Flow at Mach Number 2.5", AIAA Paper 97-3214.

Ott, P., Norryd, M., and Bölcs, A., 1998, "The Influence of Tailboards on Unsteady Measurements in a Linear Cascade", ASME Paper 98-GT-572.

Shaw, L.M., Boldman, D.R., Buggele, A.E., and Buffum, D.H., 1986, "Unsteady Pressure Measurements on a Biconvex Airfoil in a Transonic Oscillating Cascade", Journal of Engineering for Gas Turbines and Power, Vol. 108, pp. 53-59.

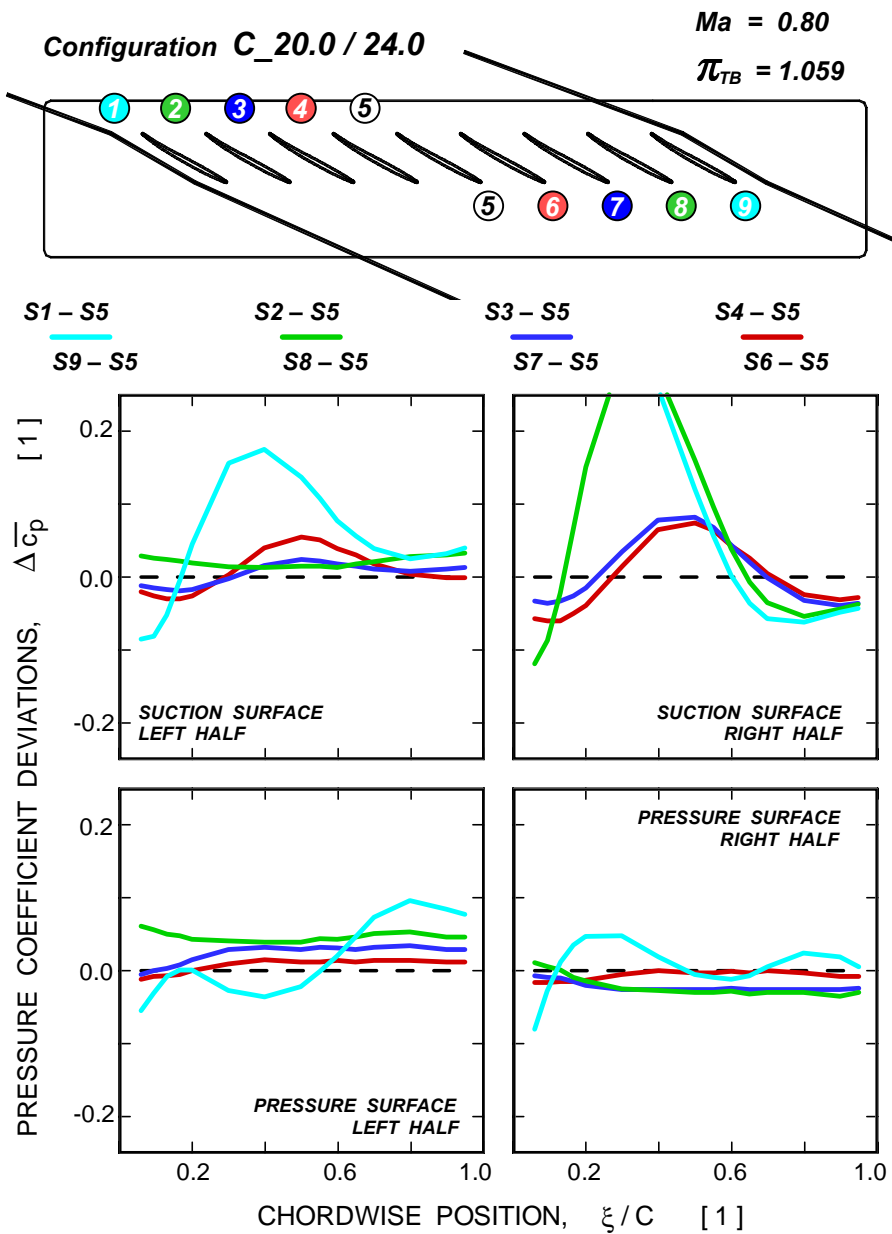Fig. 23. **Blade loading diagrams for configuration C_20.0 / 24.0**

Configuration *C_20.0 / 24.0*

*Ma = 0.80*

$\pi_{TB} = 1.059$



| S1 – S5 | S2 – S5 | S3 – S5 | S4 – S5 |
|---|---|---|---|
| S9 – S5 | S8 – S5 | S7 – S5 | S6 – S5 |

PRESSURE COEFFICIENT DEVIATIONS, $\Delta \overline{c}_p$ [1]

SUCTION SURFACE
LEFT HALF

SUCTION SURFACE
RIGHT HALF

PRESSURE SURFACE
RIGHT HALF

PRESSURE SURFACE
LEFT HALF

CHORDWISE POSITION, $\xi / C$ [1]

**Fig. 24.** **Blade loading periodicity for configuration *C_20.05 / 24.0***

BLADE FORCE, $F_B$ [N]

BLADE TORQUE, $T_B$ [Nm]

BLADE TORQUE

BLADE FORCE

BLADE NUMBER
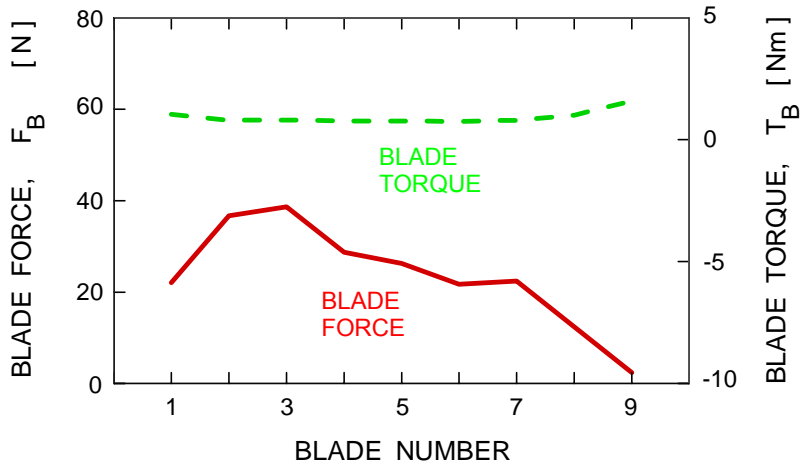
**Fig. 25.** **Distribution of blade force and torque along the cascade for configuration *C_20.0 / 24.0***

# REPORT DOCUMENTATION PAGE

| 1. AGENCY USE ONLY (Leave blank) | 2. REPORT DATE | 3. REPORT TYPE AND DATES COVERED |
|---|---|---|
| | March 2000 | Technical Memorandum |

**4. TITLE AND SUBTITLE**

On Flowfield Periodicity in the NASA Transonic Flutter Cascade,
Part I—Experimental Study

**6. AUTHOR(S)**

J. Lepicovsky, E.R. McFarland, R.V. Chima, and J.R. Wood

**5. FUNDING NUMBERS**

WU–523–26–13–00

**7. PERFORMING ORGANIZATION NAME(S) AND ADDRESS(ES)**

National Aeronautics and Space Administration
John H. Glenn Research Center at Lewis Field
Cleveland, Ohio 44135–3191

**8. PERFORMING ORGANIZATION REPORT NUMBER**

E–12179

**9. SPONSORING/MONITORING AGENCY NAME(S) AND ADDRESS(ES)**

National Aeronautics and Space Administration
Washington, DC 20546–0001

**10. SPONSORING/MONITORING AGENCY REPORT NUMBER**

NASA TM—2000-209934
ASME 2000–GT–0572

**11. SUPPLEMENTARY NOTES**

**12a. DISTRIBUTION/AVAILABILITY STATEMENT**

Unclassified - Unlimited
Subject Categories: 02 and 09          Distribution: Nonstandard

This publication is available from the NASA Center for AeroSpace Information, (301) 621–0390.

**12b. DISTRIBUTION CODE**

**13. ABSTRACT (Maximum 200 words)**

An extensive study to improve flow uniformity and periodicity in the NASA Transonic Flutter Cascade is presented here. The results are reported in two independent parts dealing with the experimental approach and the analytical approach. The first part, the *Experimental Study*, focuses first on the data sets acquired in this facility in the past and explains several discrepancies, particularly the questions of actual flow incidence and cascade backpressure levels. Next, available means for control and modifications of the cascade flowfield, boundary layer bleed and tailboard settings are presented in detail. This is followed by experimental data sets acquired in modified test facility configurations that were based on analytical predictions of the cascade flowfield. Finally, several important conclusions about improving the cascade flowfield uniformity and blade load periodicity are summarized. The important conclusions are: (1) boundary layer bleed does not improve the cascade flow periodicity; (2) tunnel wall contours must be carefully matched to the expected shape of cascade streamlines; (3) actual flow incidence for each cascade configuration rather must be measured instead of relying on the tunnel geometry; and (4) the current cascade configuration exhibits a very high blade load uniformity over six blades from blade #2 to blade #7, and the facility is now ready for unsteady pressure data acquisition.

**14. SUBJECT TERMS**

Transonic cascade testing; Cascade flow periodicity

**15. NUMBER OF PAGES**

19

**16. PRICE CODE**

A03

| 17. SECURITY CLASSIFICATION OF REPORT | 18. SECURITY CLASSIFICATION OF THIS PAGE | 19. SECURITY CLASSIFICATION OF ABSTRACT | 20. LIMITATION OF ABSTRACT |
|---|---|---|---|
| Unclassified | Unclassified | Unclassified | |